

# Magnetic Resonance Imaging Techniques for Indirect Assessment of Myelin Content in the Brain Using Standard T1w and T2w MRI Sequences and Postprocessing Analysis

Pavlína POKOŠOVÁ<sup>1,3</sup>, David KALA<sup>1,4</sup>, Jan ŠANDA<sup>2</sup>, Petr JEŽDÍK<sup>3</sup>, Yeva PRYSIAZHNÍUK<sup>1</sup>, Adéla FARIDOVÁ<sup>1</sup>, Alena JAHODOVÁ<sup>5</sup>, Anežka BĚLOHLÁVKOVÁ<sup>5</sup>, Adam KALINA<sup>6</sup>, Zuzana HOLUBOVÁ<sup>2</sup>, Bruno JURÁŠEK<sup>2</sup>, Martin KYNČL<sup>2</sup>, Jakub OTÁHAL<sup>1,4</sup>

<sup>1</sup>Department of Pathophysiology, Second Faculty of Medicine, Charles University, Czech Republic,

<sup>2</sup>Department of Radiology, Second Faculty of Medicine, Charles University and University

Hospital Motol, Prague, Czech Republic, <sup>3</sup>Faculty of Electrical Engineering, Czech Technical

University in Prague, Czech Republic, <sup>4</sup>Laboratory of Developmental Epileptology, Institute of Physiology of the Czech Academy of Sciences, Prague, Czech Republic, <sup>5</sup>Department of Pediatric Neurology, Second Faculty of Medicine, Charles University and University Hospital Motol, Prague, Czech Republic, <sup>6</sup>Department of Neurology, Second Faculty of Medicine, Charles University and University Hospital Motol, Prague, Czech Republic

Received March 31, 2023

Accepted October 10, 2023

## Summary

Magnetic Resonance Imaging (MRI) has revolutionized our ability to non-invasively study the brain's structural and functional properties. However, detecting myelin, a crucial component of white matter, remains challenging due to its indirect visibility on conventional MRI scans. Myelin plays a vital role in neural signal transmission and is associated with various neurological conditions. Understanding myelin distribution and content is crucial for insights into brain development, aging, and neurological disorders. Although specialized MRI sequences can estimate myelin content, these are time-consuming. Also, many patients sent to specialized neurological centers have an MRI of the brain already scanned. In this study, we focused on techniques utilizing standard MRI T1-weighted (T1w) and T2-weighted (T2w) sequences commonly used in brain imaging protocols. We evaluated the applicability of the T1w/T2w ratio in assessing myelin content by comparing it to quantitative T1 mapping (qT1). Our study included 1 healthy adult control and 7 neurologic patients (comprising both pediatric and adult populations) with epilepsy originating from focal epileptogenic lesions visible on MRI structural scans. Following image acquisition on a 3T Siemens Vida scanner, datasets were co-registered, and segmented into anatomical regions using the Fastsurfer toolbox, and T1w/T2w ratio maps were calculated in

Matlab software. We further assessed interhemispheric differences in volumes of individual structures, their signal intensity, and the correlation of the T1w/T2w ratio to qT1. Our data demonstrate that in situations where a dedicated myelin-sensing sequence such as qT1 is not available, the T1w/T2w ratio provides significantly better information than T1w alone. By providing indirect information about myelin content, this technique offers a valuable tool for understanding the neurobiology of myelin-related conditions using basic brain scans.

## Key words

Myelination • Magnetic resonance imaging • T1w/T2w ratio • Quantitative T1 brain mapping • Epilepsy • Focal cortical dysplasia

## Corresponding author

J. Otáhal, Department of Pathophysiology, Second Faculty of Medicine, Charles University, Plzeňská 130/221, 150 06 Praha 5, Czech Republic. E-mail: jakub.otahal@fmotol.cuni.cz

## Introduction

Myelin, a lipoprotein forming an insulating sheath around nerve axons, stands as a crucial structural

component within the nervous system. Its primary role is to augment the velocity and efficacy of signal transmission along nerve fibers. Any disruptions in myelin production or damage to the myelin sheath can precipitate a spectrum of neurological disorders, encompassing conditions such as epilepsy. Epilepsy is one of the most frequent neurological disorders, affecting approximately 1 % of the population. It is particularly frequent in infants and children in which it can lead to serious consequences later in life, such as adverse effects on brain maturation, and various cognitive deficits, especially those affecting learning and memory. The occurrence of epileptic seizures is still difficult to predict, only in some of the patients specific patterns can be identified [1]. Malformations of cortical development (MCD) and focal cortical dysplasia (FCD) in particular represent the most common cause of focal intractable epilepsy. The treatment of epilepsy is long-term and gives rise to a substantial socioeconomic load on sufferers. Current pharmacotherapies with available antiepileptic drugs (AEDs) are mostly symptomatic (anti-seizure) and in 30 % of patients not effective in obtaining complete seizure control [2]. Pharmacoresistant epilepsy thus represents a devastating disorder with significant healthcare and economic burden. In Europe, total annual direct costs are estimated to €1.698 and indirect costs to €745 per patient [2].

Epilepsy surgery is a unique hope for patients with focal intractable epilepsy. Compared with drug treatment, surgery is more likely to render patients seizure-free, off AEDs, and with a better quality of life [3]. A recent European multicenter study showed that only 57.6 % of patients with FCD were seizure-free after surgery, compared to 68.4 % of patients with tumors and 61.4 % with hippocampal sclerosis [4]. In the case of FCD, the major predictor for a favorable surgical outcome is the removal of the entire dysplastic cortex [5]. Precise presurgical delineation of FCD with the current neuroimaging and electrophysiological techniques is nevertheless challenging, primarily due to the extreme diversity of this population. FCDs exhibit typical structural alterations such as dyslamination or the presence of dysmorphic neurons, which influence contrast on common MR sequences only minimally. The currently accepted classification system divides FCD into 3 main groups and several subgroups based mainly on histological findings Blumcke [6]. Reliable localization of the dysplastic cortex is much more challenging in FCD type I; that is reflected by frequently unfavorable outcomes of surgery in this group of patients [7].

Despite prominent progress in neuroimaging techniques, particularly MRI, delicate alterations of brain tissue in epileptogenic lesion is hard to detect with conventional approaches. It has been shown recently that in part of originally diagnosed “non-lesional” epilepsies was a “lesion” identified later with more advanced imaging approaches [8]. Dysplastic tissue can be detected by MRI only in situations where it possesses distinct properties from surrounding tissue. Although changes in microscopic structure are visible on histology, FCDs, especially of type I and small type II are difficult to detect with the use of the common MRI approaches [9]. However, altered myelination has been repeatedly observed in resected human FCD tissue. Hypomyelination was more prominent in FCDs with dysmorphic cells but visible in all types of FCDs [10,11].

Conventional MRI sequences are, however, not specific for directly assessing myelin content in the brain. While designated MRI sequences have shown promise in assessing myelin content with various specificities [12], they are not widely available on common MR scanners and require experienced staff, also significantly extend scanning protocols and potentially affect the overall yield of the MR examination, especially in pediatric epilepsy patients.

Thus, there is a need for a routine indirect myelin content assessment method that can utilize standard MRI sequences, which are already included in designated epilepsy MR protocols and are routinely used for the initial examination of epilepsy patients even before referral to a specialized epilepsy center [13]. It's important to highlight that T1w and T2w sequences generally offer qualitative insights into myelin distribution in the brain. Consequently, alternative MRI techniques are favored to compare myelin levels [14]. The T1w/T2w ratio can provide information about tissue contrast and can be used to indirectly assess myelin content in the brain [14-17]. Higher myelin content generally leads to a higher T1w/T2w ratio, as myelin-rich white matter tends to have a higher T1 signal and a lower T2 signal [14].

In this study, we investigated whether lateral differences exist in the intensity of myelin-sensitive MRI sequences in patients with focal epilepsy, whether lateral changes in volume are accompanied by changes in the intensity of these sequences, whether T1w/T2w correlates with qT1 sequence used previously for MRI detection of myelin, and whether T1w/T2w can be used as a full replacement for qT1 in patients with focal epilepsy.

## Methods

In this study, we investigated 7 patients diagnosed with focal epilepsy, who were enrolled in the epileptosurgery program at Motol Hospital. Additionally, we included 1 healthy adult for comparison. All participants underwent thorough evaluations using a specially designed epilepsy MRI protocol [17], comprising high-resolution anatomical scans, quantitative T1 mapping, and diffusion kurtosis imaging (DKI) sequence. The research protocol received ethical approval from the Ethics Committee of University Hospital Motol, and informed consent was obtained from all participating patients.

### Participants

Subject A is a 46-year-old male with histologically confirmed FCD type 2b in the left hemisphere. The MRI scans show cortical thickening and signal alteration at the base of the left paracentral sulcus. The cortex appears slightly brighter than usual in T1w images and brighter in T2w images. Additionally, there is blurring of the white/gray matter interface. Based on the MR findings, FCD type 2b is suspected.

Subject B is a 6-year-old female with histologically confirmed FCD type 2b in the left hemisphere. The MRI scans reveal cortical thickening and signal alterations at the base of the precentral sulcus on the left. The cortex appears hyperintense in T2w/FLAIR images and hypointense in T1w images. Additionally, there is a blurring of the white-gray matter interface. While changes in the transmantle pattern cannot be excluded. FCD type 2b is suspected based on the MRI findings.

Subject C is a 3-year-old male with a histologically confirmed dysembryoplastic neuroepithelial tumor (DNET) in the right hemisphere. The lesion is situated cortically in the frontal region on the right, measuring up to 1.0 cm in size. It appears inhomogeneously hyperintense with a hypointense center in T2w images and hypointense in T1w images. Additionally, there is a moderate signal in FLAIR images, and focal areas exhibit a discontinuous layer of cortex. Radiologically, the images suggest the possibility of either a glioneuronal cyst or a dysembryoplastic neuroectodermal tumor.

Subject D is a 3-year-old male diagnosed with MCD in the left hemisphere. Extensive, diffuse juxtacortical white matter signal changes are observed in the left frontal lobe, insular area, and temporal lobe, with extension into the left parietal lobe. Additionally, there is a blurring of the grey and white matter interface, raising suspicion of atypia of

gyrification in these regions. The cortex appears slightly hyperintense in T2w/FLAIR images, while T1w images show no cortical signal alteration. The juxtacortical white matter appears hyperintense in T2w and FLAIR images, with overall mild white matter reduction. Radiologically, the pattern suggests extensive malformation of cortical development in the left cerebral hemisphere.

Subject E is an 18-year-old female with a diagnosed FCD type 1a in the right hemisphere. MRI findings reveal extensive and diffuse white matter signal changes in the right frontal region, predominantly ventrally with the most significant alterations observed mesially. The signal appears hyperintense in T2w/FLAIR images, accompanied by a reduction in white matter volume. These changes are distributed diffusely and result in a blurring of the grey and white matter interface. Subcortical white matter changes are mildly hypointense in T1w images, with no apparent gyration atypia. Most likely, these changes are consistent with extensive focal cortical dysplasia type 1 affecting the ventral and ventromedial portions of the right frontal lobe, overlapping into the anterior insular area on the right.

Subject F is a 56-year-old male with a confirmed diagnosis of FCD type 2b in the right hemisphere. The MRI shows atypical gyration of the cingulate gyrus ventrally in the right mesial frontal region, accompanied by a mild thickening of the cortex and blurring of the gray/white matter interface. The juxtacortical white matter appears mildly hyperintense in T2w/FLAIR images and hypointense in T1w images. Additionally, the cortex exhibits diffuse high signal intensity in T2w/FLAIR images. These findings raise radiological suspicion of focal cortical dysplasia type 2b.

Subject G is a 5-year-old male with a confirmed diagnosis of MCD in the left hemisphere. The MRI revealed an extensive expanding area in the left frontal lobe, extending beyond 6.6 cm ventrodorsally, with a small impression on the adjacent frontal skull. The cortical and subcortical white matter changes appear irregularly hyperintense in FLAIR with some hypointense portions, and they show inhomogeneous hyperintensity in T2w images, mostly appearing hypointense in T1w sequences. The boundary with the surrounding white matter is markedly multilobulated. Based on the radiological findings, a glioneuronal lesion or DNET was suspected.

The control subject is a 58-year-old male who underwent MRI scans of the left hip due to persistent arthralgia. There are no neurological symptoms or pathological findings observed on the brain MRI scans.

Representative MRI scans are provided in Figure 1.

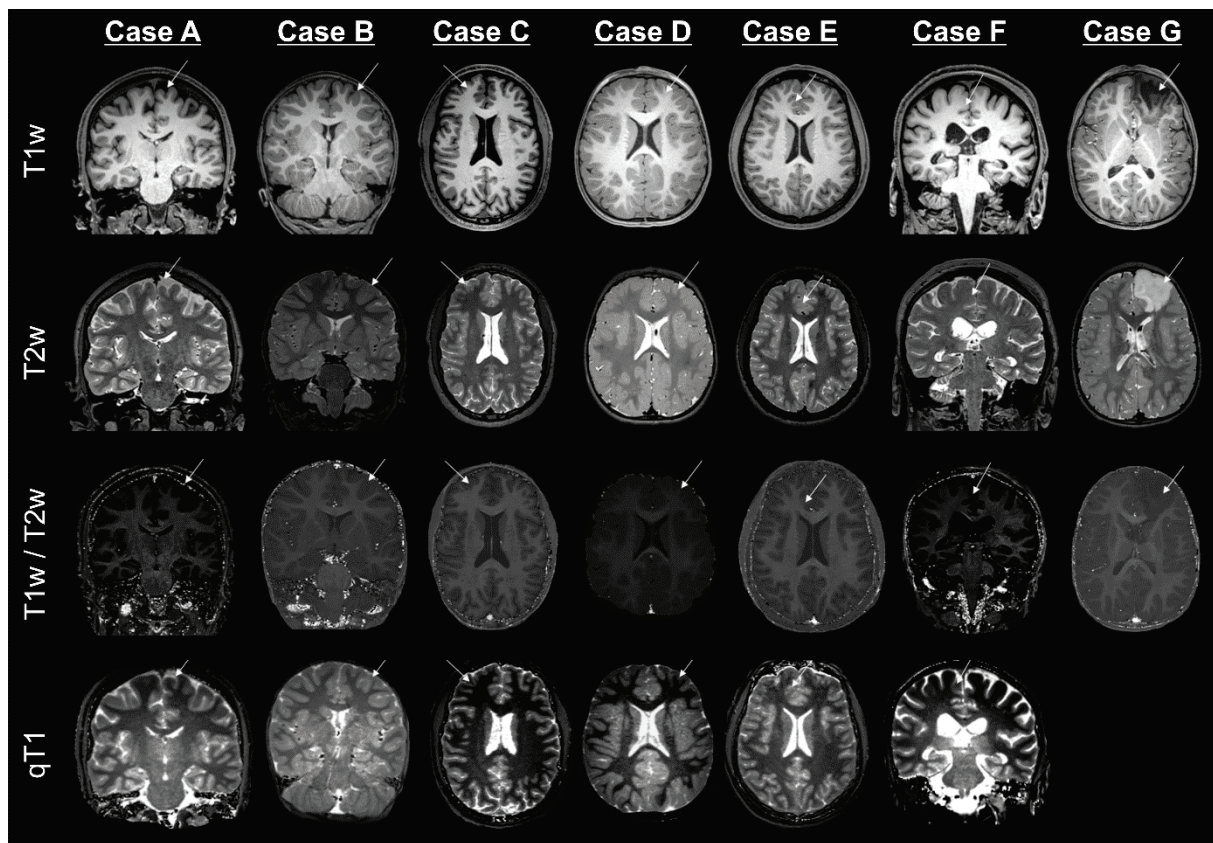


**Fig. 1.** Representative images from the obtained MRI dataset for each subject. Arrow indicates observed epileptogenic lesion.

#### MRI acquisition

MRI examination was performed in Motol University Hospital using a Siemens 3T Vida Magnetom scanner with the 64-channel head coil. Designated epilepsy MRI protocol [17] includes both structural and diffusion sequences. T1-weighted (T1w) images were acquired using a 3D MP-RAGE sequence, with repetition time TR 2400 ms, echo time TE 2.29 ms, flip angle FA 8°, acquisition matrix 0.8×0.8×0.8 mm, orientation sagittal, interpolation factor 2, voxel size .4×0.4×0.8 mm, averaging 1, acceleration GRAPPA factor 2, and duration 6:47 min. T2-weighted (T2w) dataset was recorded with 3D SPACE sequence with repetition time TR 3200 ms, TE 572 ms, TSE with variable flip angle of refocusing RF pulses (details are in [18]), acquisition matrix 0.8×0.8×0.8 mm, orientation sagittal, interpolation factor 2, voxel size 0.4×0.4×0.8 mm, averaging 1.8, acceleration CAIPIRNHA factor 3, and duration 6:35 min. Acquisition of Fluid Attenuation Recovery (FLAIR) was performed using 3D SPACE sequence with repetition time TR 6000 ms, TE 350 ms, TI 1900 ms, variable FA, acquisition matrix 1×1×0.9 mm, orientation sagittal, interpolation factor 2, voxel size 0.5×0.5×0.9 mm, averaging 1.8, acceleration CAIPIRNHA factor 4, and

duration 8:02 min. Quantitative T1 (qT1) map was measured by the method of two variable flip angles, gradient echo sequence, TR 15 ms, TE 2 ms, FA 4° and 23°, acquisition matrix 1×1×1 mm, orientation sagittal, interpolation factor 2, voxel size 0.5×0.5×1 mm, averaging 1, acceleration GRAPPA factor 2, and duration 8:45 min. Diffusion MRI (DWI) was acquired with EPI sequence, repetition time TR 5300 ms, TE 97 ms, acquisition matrix 2×2×2 mm, orientation transversal, no interpolation, voxel size 2×2×2 mm, b 0, 1000, and 3000 s/mm<sup>2</sup>, in 20 directions, averaging 1, acceleration SMS factor 3, and duration 4:42 min. For distortion correction additional + 5 b0 images with PA phase encoding direction and 5 b0 images in AP direction were also acquired.

#### MRI preprocessing

We performed registration of all MRI sequences to the common anatomical space of the T1w image. Subsequently, we normalized them into the standard MNI (Montreal Neurological Institute template) space. During the normalization process, we carefully removed all non-brain structures, including the skull, muscles, skin, and cerebral fluid. Registration and normalization were

performed using the SPM12 MATLAB toolbox.

#### Segmentation

To segment the brain into specific regions of interest, we utilized FastSurfer, a fast and accurate deep-learning-based neuroimaging pipeline [19]. This open-source software is optimized for rapid and precise anatomical brain segmentation, including surface reconstruction and cortical parcellation. The computational time for segmentation varied, taking up to two hours depending on the MRI dataset's quality. For enhanced segmentation quality in pediatric patients, we employed the Infant tool, which considers incomplete brain development [19,20].

Within volumetric comparison, our focus was on

the following structures: cerebral white matter, lateral ventricle, thalamus, caudate, putamen, pallidum, hippocampus, amygdala, ventral diencephalon, and cortex of individual brain lobes, including frontal, parietal, temporal, occipital, cingulate, and insula. For signal intensity comparison in anatomical regions, we selected the following regions of interest for further analysis: whole hemisphere, white matter, whole cerebral cortex, individual brain lobes – frontal, parietal, temporal, occipital, cingulate, and insula, lateral ventricles, and subcortical grey matter – thalamus, ventral diencephalon, hippocampus, nucleus pallidum, caudate, putamen, amygdala, and accumbens. The segmentation results and individual regions of interest (ROI) are illustrated in Figure 2.

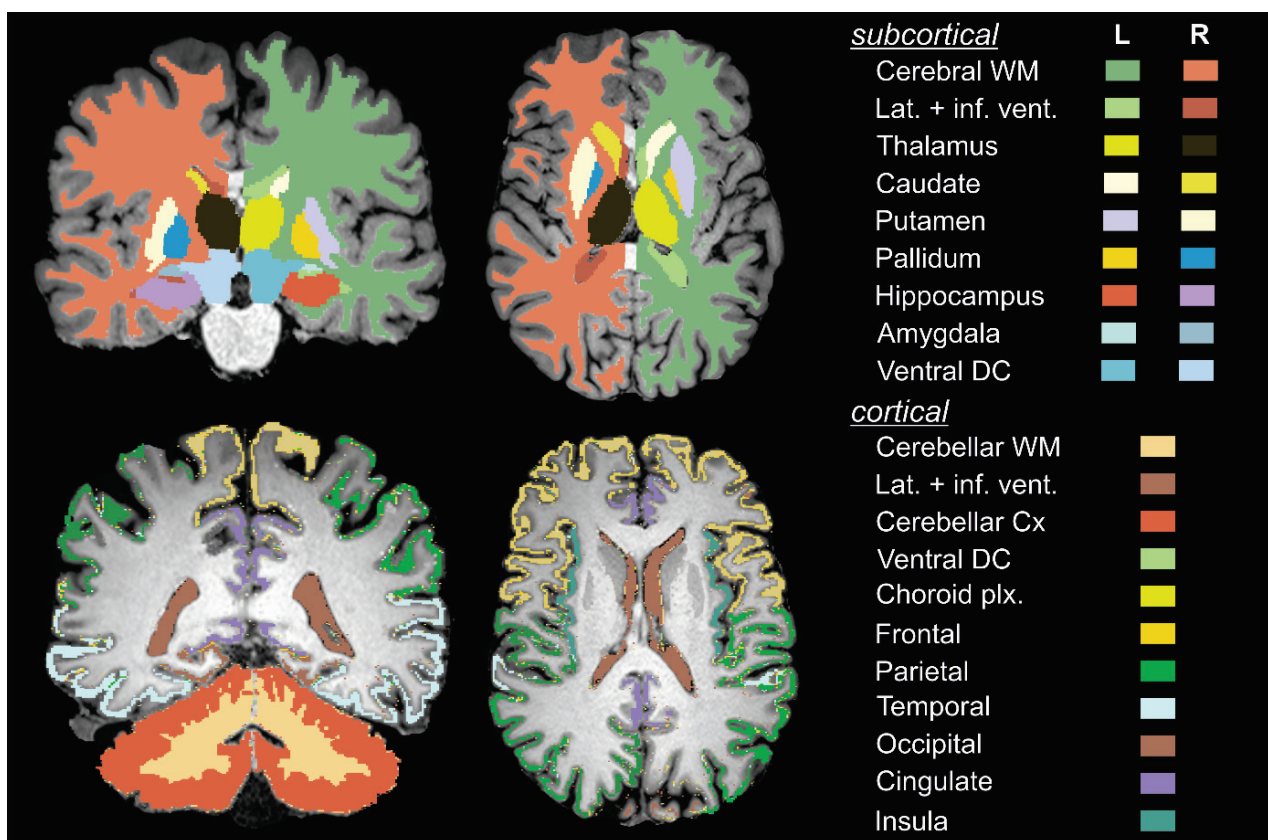


**Fig. 2.** – Segmentation masks for the selected regions as a result of segmentation using T1w datasets with the FastSurfer pipeline.

#### Statistics

Data were processed and statistically evaluated using in-house Matlab software (Mathworks, Natick, USA). Non-parametric tests (Wilcoxon signed rank test) with a level of statistical significance of 5 % have been used. The non-parametric correlation coefficient Spearman's  $r$  was chosen due to the non-normality of the distribution of both variables. In this study, hemispheres

and their subregions (Fig. 2) were compared in the matter of their volumes and intensities of T1w/T2w ratio and qT1. Absolute (absolute diff) and relative difference (relative diff) were calculated according to equations 1 and 2, respectively.

$$\text{Absolute diff [a.u.]} = \text{ipsi [a.u.]} - \text{contra [a.u.]} \quad \text{eq. 1}$$

$$\text{Relative diff [%]} = \frac{\text{ipsi [a.u.]} - \text{contra [a.u.]}}{\text{contra [a.u.]}} \cdot 100 \quad \text{eq. 2}$$

## Results

All participants successfully underwent MRI scanning, and the entire dataset was acquired except for subject G, where the qT1 was not obtained with the desired quality. Figure 1 displays representative images from the obtained MRI dataset for each subject. We chose the orientation that is most suitable for displaying the pathology. The segmentation using T1w datasets with the FastSurfer pipeline was successful for all subjects, and we obtained segmentation masks for the selected regions, as shown in Figure 2.

Following the segmentation, we proceeded to assess volume changes. To evaluate the overall symmetry of the brain hemispheres, we assessed volumes of individual hemispheres together with the volume of ipsilateral and contralateral grey matter, white matter, and lateral ventricles and conducted pairwise (ipsilateral versus contralateral) comparisons. Since patient F, who has a diagnosed FCD type 2b, has exceptionally large ventricular volumes that could affect the statistics, we decided to exclude this patient from this part of the analysis (Table 1). None of the analyzed segments showed significant volume variation according to the Wilcoxon matched-pairs test. However, volume alterations in the lateral ventricle in the ipsilateral hemisphere were observed in all six analyzed patients (mean volume of 6817 mm<sup>3</sup> in ipsilateral versus 5853 mm<sup>3</sup>). The relationship between volumes of brain lateral ventricles for individual patients is illustrated in Figure 3, where excluded outlier patient F can also be seen. We assessed this relationship using the non-parametric Spearman's correlation coefficient for six patients (patient F excluded). Although a mean positive dependence of 0.31 between ipsilateral and contralateral ventricle volumes was observed, the low number of cases did not result in statistical significance. To explore potential volume alterations of other brain structures, we conducted a detailed volume comparison of the regions of interest (ROIs) segmented using FastSurfer. We calculated both absolute and relative differences between the ipsilateral and contralateral volumes for all ROIs (Cerebral white matter, Lateral ventricle + Inferior lateral ventricle, Thalamus, Caudate, Putamen, Pallidum, Hippocampus, Amygdala, Ventral DC, Frontal cortex, Parietal cortex, Temporal cortex, Occipital cortex, Cingulate, and Insula) (Table 2).

To reveal alterations in myelin content within segmented brain structures we focused on T1 relaxation since myelin shortens T1 relaxation time, allowing it to quickly recover its equilibrium magnetization after being disturbed. As a result, regions with higher myelin content

appear brighter on T1w MRI images, while regions with less myelin appear darker. However, it is important to note that T1w MRI sequences offer only indirect information about myelin content and cannot quantitatively measure the exact amount of myelin in a specific region. Additionally, T1w images are sensitive to various other effects arising from the tissue itself and scanner inhomogeneities. To address these considerations, we calculated the voxel-based T1w/T2w ratio on co-registered images to evaluate its validity for a better, yet still indirect, estimation of myelin content [21]. Intensities of the T1w/T2w ratio and qT1 were calculated for each ROI and compared by means of side differences in Table 3 and Table 4, respectively. Both tables provide data on absolute and relative differences in intensities (T1w/T2w) or T1 relaxation times (qT1) for all subjects and ROIs. Additionally, we explored whether the values observed in T1w/T2w and qT1 correlate with each other, with the aim of determining if T1w/T2w ratio images could serve as a substitute for qT1 images. We calculated the pairwise Pearson's correlation coefficient between T1w/T2w ratios and qT1 values, considering data from all voxels within the brain tissue, whether white or grey matter. The correlation coefficients for all subjects are presented in Table 5. Moreover, Figure 4 depicts detailed correlation plots for Subject A. We observe the most robust correlation in patient A, characterized by a value of -0.5. Conversely, the weakest correlation is found in patient F, registering at 0.06 (Table 5). Unfortunately, the sequence of qT1 images for patient G could not be used due to low image quality.

To gain deeper insights into the T1w/T2w ratio, we utilized a control healthy subject and conducted a comprehensive intensity analysis of all sequences within the designated epilepsy protocol. We generated polar plots, illustrating absolute and relative side differences, and employed Cohen's D effect size to compare left/right ROIs for each sequence (Fig. 5A-C). The intensity analysis revealed a clear distinction between T1w and qT1 values. Consequently, we constructed histograms comparing ipsilateral and contralateral voxel intensities of ROIs (Fig. 5D-E). While the histograms of qT1 values perfectly matched each other, the T1w histograms displayed a significant shift in distributions, albeit not attributed to a T1 effect. The shift can be a result of magnetic field inhomogeneity within the scanner. However, upon the division of T1w by T2w (T1w/T2w ratio), the two distributions (ipsilateral and contralateral) showed remarkable overlap, similar to qT1 (Fig. 5F). This suggests that the T1w/T2w ratio effectively mitigates the intensity variations observed in T1w images.

**Table 1.** Mean of absolute volumes for different brain structures with its standard deviation and standard error of the mean.

		Mean [ml]	Std. Deviation [ml]	Std. Error Mean [ml]
<i>Ventricles</i>	Ipsi	6.8	1.9	0.8
	Contra	5.9	2.5	1.0
<i>Whole hemisphere</i>	Ipsi	456.9	6.9	28.1
	Contra	466.9	84.9	34.7
<i>GM</i>	Ipsi	257.3	51.8	21.1
	Contra	268.6	51.8	21.1
<i>WM</i>	Ipsi	208.6	53.7	21.8
	Contra	212.9	51.8	21.1

**Table 2.** The absolute difference [ml] and relative difference [%] of the volumes of individual regions of interest on a given hemisphere. Negative values highlighted with an orange background indicate lower volume of ipsilateral ROI.

Patient	The absolute (ml) and relative (%) change of volume of ROIs						
	A	B	C	D	E	F	G
<i>Whole hemisphere</i>	-8.1 (-1.4)	0.1 (0)	6.3 (1.3)	-30.2 (-7.7)	-0.5 (-0.1)	36.1 (7.6)	-15.3 (-2.9)
<i>Cerebral white matter</i>	-3.2 (-1.1)	-0.1 (-0.1)	-4 (-1.7)	-11.2 (-7.8)	-2.8 (-1.6)	13.3 (5.7)	-5.1 (-2.6)
<i>Lateral Ventricle + Inferior</i>	4.1 (96.7)	2.3 (79.2)	-1.3 (-14.1)	0.5 (10.8)	-0.3 (-6.8)	2.2 (8.7)	0.5 (9)
<i>Thalamus</i>	0 (-0.5)	0.1 (1)	-0.1 (-1.7)	-0.3 (-4.1)	0.1 (0.9)	-0.5 (-7.3)	0.1 (1.7)
<i>Caudate</i>	-0.2 (-8.2)	0 (0.5)	0.2 (5)	0.1 (2.2)	0.2 (6)	0.3 (10.6)	-0.1 (-3.6)
<i>Putamen</i>	-0.1 (-1.8)	-0.1 (-2)	0.1 (1.2)	0 (-0.8)	-0.1 (-1.8)	0.2 (3.5)	0.4 (7.2)
<i>Pallidum</i>	0.1 (5.3)	0.3 (22.2)	-0.2 (-7.4)	0.2 (17.9)	-0.3 (-14.5)	0 (-2.1)	0.1 (4.1)
<i>Hippocampus</i>	-0.4 (-8.7)	0 (-1.3)	0.3 (8.7)	-0.1 (-3)	-0.1 (-2.8)	0.2 (4.8)	0.2 (5.7)
<i>Amygdala</i>	0 (-1.1)	-0.6 (-26.9)	0.2 (9.7)	-0.4 (-19.3)	0.3 (21.3)	0.2 (10.6)	-0.4 (-19.1)
<i>Ventral DC</i>	0.4 (8)	-0.1 (-3.3)	-0.3 (-5.5)	-0.2 (-8)	-0.1 (-2.8)	0 (1.1)	0.1 (3.7)
<i>Frontal</i>	-4.2 (-5)	-5.7 (-10.7)	1.1 (1.4)	0 (0.1)	1.4 (2.6)	3.5 (5.2)	-0.7 (-1)
<i>Parietal</i>	2.5 (4.2)	-1 (-2.5)	0.6 (1.4)	-5.7 (-18.7)	0.2 (0.6)	4.7 (9.8)	-0.1 (-0.3)
<i>Temporal</i>	-0.4 (-0.8)	-0.9 (-3.4)	-2 (-5.6)	-1.2 (-5.6)	-1.3 (-4.8)	1 (2.6)	1.1 (3.8)
<i>Occipital</i>	-3.6 (-10.3)	2.8 (17.3)	0.6 (2.4)	1.1 (9.8)	0 (-0.2)	5.7 (23.6)	0.7 (3.5)
<i>Cingulate</i>	3.7 (21.1)	3.4 (32.6)	-3.3 (-19.3)	2.7 (30.1)	-3 (-22)	2.5 (12.6)	3.5 (26.4)
<i>Insula</i>	-0.6 (-6.1)	-0.4 (-5)	0.4 (5.3)	0.2 (2.5)	0.5 (9)	0.3 (3.7)	-0.7 (-10.3)

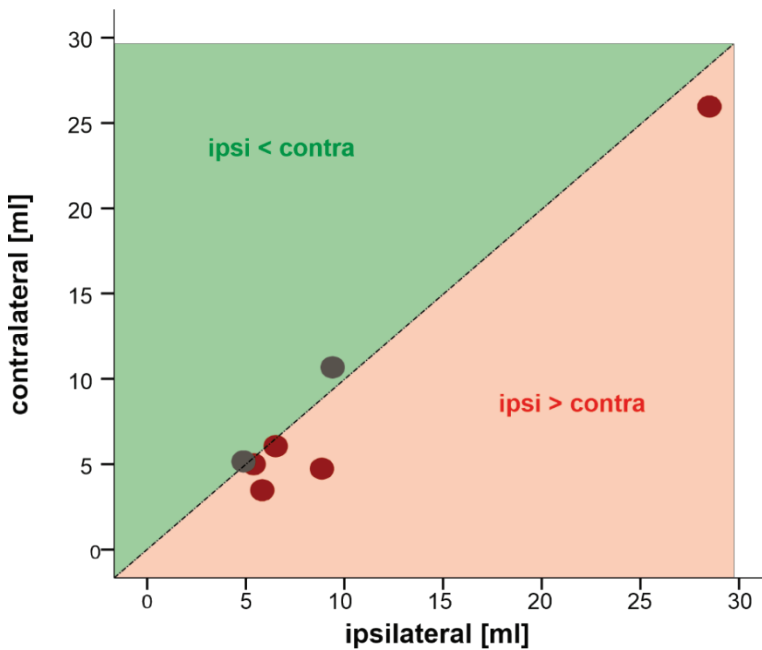


**Fig. 3.** Relation of the volumes of ipsilateral and contralateral ventricles.

**Table 3.** Absolute differences of intensities [a.u.] of segments and in parentheses relative differences of segments [%] for T1w/T2w images.

Patient	Absolute difference of intensity [a.u.] for segments and relative difference [%] for T1w/T2w images						
	A	B	C	D	E	F	G
<i>Ganglia</i>	0.042 (1.4 %)	0.101 (4.96 %)	-0.113 (-4.34 %)	-0.003 (-21.74 %)	-0.028 (-1.14 %)	-0.215 (-7.87 %)	0.0562 (2.8 %)
<i>WM</i>	-0.137 (-3.73 %)	-0.008 (-0.32 %)	0.054 (1.64 %)	-0.001 (-7.34 %)	-0.099 (-3.24 %)	-0.301 (-9.84 %)	-0.088 (-4.1 %)
<i>Frontal</i>	-0.006 (-0.33 %)	-0.008 (-0.58 %)	0.012 (0.75 %)	-0.094 (-56.34 %)	0.002 (0.11 %)	-0.054 (-2.97 %)	-0.015 (-1.2 %)
<i>Parietal</i>	-0.090 (-4.85 %)	0.007 (0.54 %)	0.065 (3.89 %)	-0.001 (-6.21 %)	0.006 (0.39 %)	-0.067 (-3.49 %)	-0.017 (-1.3 %)
<i>Temporal</i>	-0.067 (-3.98 %)	0.002 (0.17 %)	0.031 (1.98 %)	-0.001 (-2.41 %)	0.031 (2.06 %)	-0.014 (-0.78 %)	-0.015 (-1.1 %)
<i>Occipital</i>	-0.120 (-5.53 %)	-0.080 (-4.78 %)	0.079 (3.84 %)	-0.001 (-11.71 %)	0.083 (4.70 %)	0.034 (1.54 %)	-0.015 (-1.2 %)
<i>Insula</i>	-0.047 (-2.78 %)	0.033 (2.39 %)	0.014 (0.88 %)	-0.001 (-8.28 %)	0.038 (2.52 %)	0.017 (1.05 %)	-0.014 (-1.1 %)
<i>Cingulate</i>	-0.020 (-1.15 %)	-0.003 (-0.21 %)	-0.025 (-1.54 %)	-0.001 (-5.58 %)	0.004 (0.24 %)	-0.107 (-5.95 %)	-0.014 (-1.1 %)

**Table 4.** Absolute differences of relaxation times [ms] of segments and in parentheses relative differences of segments [%] for qT1.

Patient	Absolute difference of relaxation time [ms] for segments and relative difference [%] for qT1 images					
	A	B	C	D	E	F
<i>Ganglia</i>	-72 (-3.74 %)	67 (3.27 %)	36 (2.04 %)	-325 (-11.51 %)	64 (3.43 %)	460 (24.55 %)
<i>WM</i>	-90 (-7.15 %)	44 (3.11 %)	118 (9.39 %)	-23 (-1.18 %)	63 (4.49 %)	-64 (-3.478 %)
<i>Frontal</i>	38 (2.76 %)	118 (8.17 %)	-71 (-5.80 %)	7 (0.39 %)	20 (1.41 %)	-62.5 (-4.88 %)
<i>Parietal</i>	-170 (-10.08 %)	92 (5.19 %)	203 (14.21 %)	24 (1.13 %)	33 (2.13 %)	-2 (-0.13 %)
<i>Temporal</i>	-140 (-7.36 %)	39 (2.16 %)	199 (10.69 %)	-113 (-5.17 %)	53 (2.77 %)	64 (3.97 %)
<i>Occipital</i>	-279 (-12.21 %)	-60 (-2.76 %)	328 (16.33 %)	-271 (-11.18 %)	129 (6.23 %)	-260 (-11.75 %)
<i>Insula</i>	-122 (-5.48 %)	285 (13.95 %)	193 (9.94 %)	-24 (-0.94 %)	33 (1.49 %)	-545 (-27.53 %)
<i>Cingulate</i>	-68 (-3.28 %)	-155 (-7.07 %)	-95 (-5.28 %)	-304 (-11.38 %)	4 (0.21 %)	164 (12.81 %)

**Table 5.** Correlation coefficients between the T1w/T2w ratio and qT1 images for whole hemispheres, white and grey matter respectively.

Patient	r [Whole brain]	R [WM]	R [GM]
A	-0.50363	-0.21399	-0.16285
B	-0.35188	-0.21294	0.09450
C	-0.38291	-0.25875	-0.05321
D	-0.21764	-0.14513	-0.28148
E	-0.34135	-0.24584	-0.00391
F	0.05710	0.03333	0.05871

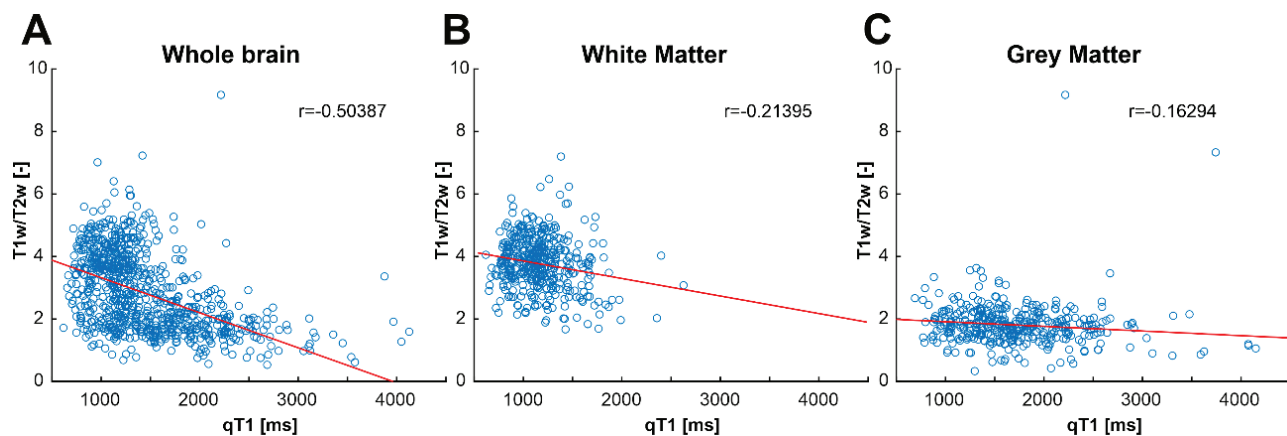


**Fig. 4.** Correlation plot for qT1 and T1w/T2w in Subject A.

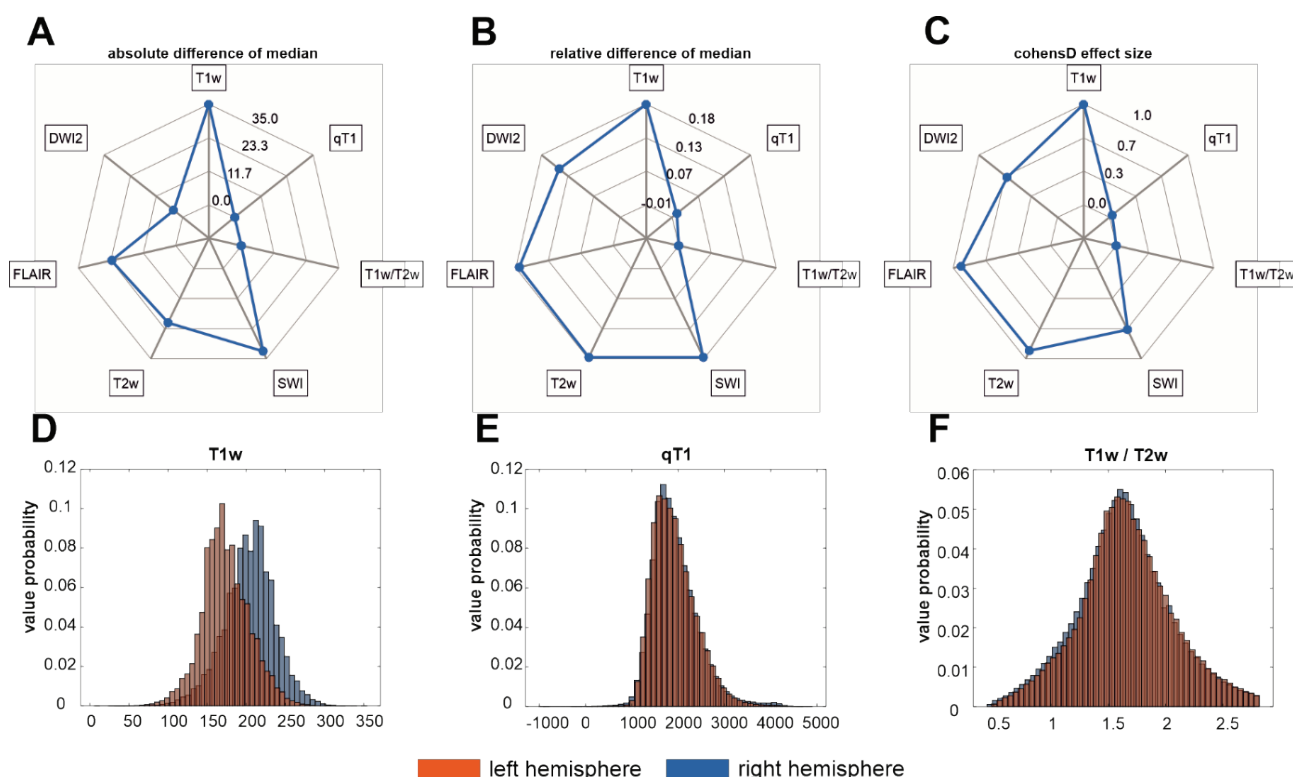


**Fig. 5.** Polar plots, illustrating absolute and relative side differences, and Cohen's D to compare the left/right temporal cortex for each sequence in the control subject (A-C). Histograms comparing voxel intensities of left and right temporal cortex in the control subject (D-F).

## Discussion

The non-invasive assessment of myelin content within the brain plays a pivotal role in understanding neurodevelopmental processes and neurological disorders. We investigated the potential of standard T1w and T2w MRI sequences, commonly employed in brain MRI protocols, for indirect estimation of myelin content. We focused on utilizing the T1w/T2w ratio as a simple yet promising method to gauge myelin levels and compared its applicability to quantitative T1 mapping (qT1) in both patients with focal epilepsy and healthy adult control. This study specifically aimed to discern whether there are lateral variations in the intensity of myelin-sensitive MRI sequences in patients with focal epilepsy. We also investigated whether changes in volume are associated with alterations in the intensity of these sequences. Furthermore, we explored the correlation between the T1w/T2w ratio and the previously utilized qT1 sequence for MRI-based myelin detection. Lastly, we examined the viability of using the T1w/T2w ratio as a comprehensive substitute for qT1 in focal epilepsy patients.

To address whether lateral differences exist in the intensity of myelin-sensitive MRI sequences in patients with focal epilepsy T1w and T2w together with qT1 sequences were employed. Standard MRI sequences such as T1w and T2w have been widely used for brain imaging due to their routine inclusion in clinical protocols, enabling comprehensive neuroanatomical assessment. However, T1w images are susceptible to various artifacts arising from both the MRI scanner and biological sources. Magnetic field inhomogeneity, a common source of such artifacts, can lead to disparate image intensities in mirror regions, i.e. homologous regions in the contralateral hemisphere. This discrepancy poses a challenge for accurate diagnosis and automatic segmentation, potentially resulting in erroneous conclusions or false-positive detections. To address this concern, we explored two main approaches: voxel-wise T1w/T2w ratio and quantitative T1 mapping. The calculation of the T1w/T2w ratio on co-registered images aims to both mitigate the impact of magnetic field inhomogeneity and to increase myelin contrast [14,22]. Our investigation in healthy control subjects revealed a significant improvement in the alignment of the intensity distribution of the T1w/T2w ratio compared to the original T1w (Fig. 5). Additionally, we generated a quantitative T1 map calculating T1 relaxation times

from two consecutively scanned T1w images with different flip angles. Another approach exists providing similar results based on T1w scans with two or more repetition times [23]. Regardless of the method by which the quantitative T1 maps were obtained they offer a direct representation of T1 relaxation times, with minimal influence from magnetic field inhomogeneity. In our study, we present both T1w/T2w ratio and quantitative T1 MRI modalities to indirectly assess the myelin content within the brain. Remarkably, the T1w/T2w ratio exhibited a high degree of similarity to qT1, indicating that it captures purified T1 information relevant to myelin content [23]. Both approaches were used to assess signal alteration in brain regions of subjects with focal epilepsy due to the presence of unilateral epileptogenic lesions. Table 3 and Table 4 present data derived from intensity images generated by the T1w/T2w ratio and qT1 sequences. Our initial focus was on larger-volume anatomical units, specifically the subcortical white matter, which encompasses the cerebral cortex and cerebral white matter. No significant changes were observed on both T1w/T2w and qT1 datasets. Additionally, we conducted comparisons of signal intensities in homologous regions and identified minor signal alterations within the ipsilateral cortex. However, due to the limited number of subjects and their heterogeneity, we were unable to perform statistical analysis on these signal changes. In our cohort, we observed radiologically suspected malformations of cortical development including focal cortical dysplasias or tumors associated with long-term epilepsy (LEATs). Within this group gangliogliomas and dysembryoplastic neuroepithelial tumors (DNET) predominates. LEATs are further united by cytoarchitectural changes that may be present in the adjacent cortex which have some similarities to developmental focal cortical dysplasias (FCD). These are now grouped as FCD type IIIb in the updated International League Against Epilepsy (ILAE) classification [24]. Regarding the myelin content of epileptogenic lesions, we analyzed signal alterations within regions rather than directly within the lesion itself. However, it is noteworthy to mention that DNET, in particular, exhibits T1 signal alterations due to the presence of oligodendrocyte-like cells (OLCs) expressing myelin oligodendrocyte glycoprotein, resulting in compromised myelination. Consequently, DNET is typically hypointense on T1w imaging compared to adjacent brain tissue [24].

Our next aim was to elucidate whether lateral

differences in the volume of the structures are accompanied by changes in the intensity of myelin-sensitive sequences. First, we found a significant decrease in the volume of the ipsilateral hemisphere, accompanied by a corresponding volume increase of the lateral ventricle in the brain. These volume alterations are mainly due to the decreased volume of the grey matter of the ipsilateral hemisphere while the white matter remains almost unaffected (Tables 1 and 2). However, it is essential to acknowledge that in some cases, FastSurfer excluded LEATs from segmentation, leading to a calculated decrease in the hemisphere's volume and adjacent structures. Conversely, the volume of the ipsilateral ventricles increased, suggesting a general atrophy of the ipsilateral hemisphere. It is worth to mention that lateral ventricles volume was still within the physiological range for the corresponding age [25]. Additionally, we conducted an examination of the volume distribution within each subcortical and cortical segment. Comparing relative differences of the volume of individual segments within the specified hemisphere in Table 2, we can identify, that alteration in hemispherical volume is caused rather by general atrophy affecting the entire hemisphere than by atrophy of specific structures.

We were further interested in whether the T1w/T2w ratio correlates with intensities of qT1 sequence which has been widely used previously for MRI detection of myelin. First, we calculated correlation coefficients of voxel-wise pairs of T1w/T2w values and qT1 intensities within the whole brain, grey and white matter within patients with focal epilepsy. Table 5 provides correlation coefficients for all subjects while Figure 4 shows the graphical interrelation of the T1w/T2w ratio with qT1 signal for a single subject (subject A). We have observed a good correlation between the T1w/T2w ratio with qT1 in all subjects except Subject F. Although Subject F, like Subject A, has been classified and histologically confirmed as having FCD type IIb they behave differently. Subject F has an extensive alteration in cortical gyration and radiologically described diffuse T2w hyperintensity of the cortex. The signal in all three modalities was increased when compared to Subject A and enlarged ipsilateral lateral ventricle which altogether indicates widespread diffuse hemispherical pathology. However, we have not found a trustworthy explanation for this mismatch in the otherwise reasonable correlation pattern (Table 5).

In our study, we employed the T1 effect as an

indirect measure of myelin content within the brain. This approach has been widely used in numerous studies to evaluate myelin changes [14]. However, it is essential to acknowledge that T1 alterations can be influenced by various sources, extending beyond myelin content [24]. T1, primarily reflecting the mobility of molecules, particularly water protons, and their binding to macromolecules, is a valuable tool for assessing macromolecular content, water binding, and water content in diverse pathologies, including conditions involving altered myelin content and inflammation [23]. While more sensitive and specific MRI sequences have been developed and tested for myelin assessment (for a comprehensive review see [26]), our intent was to utilize common sequences that are routinely available in every brain scan conducted during the epilepsy diagnosis process. The overall time required for the diagnostic protocol is critical, especially in pediatric patients, where general anesthesia is not recommended. Typically, the scanning duration approaches approximately one hour, which can be challenging for these young patients to endure [27]. Consequently, even if specialized myelin-specific sequences are available onsite, their utilization is often precluded due to the extended examination time. In our investigation, we sought to address this constraint by demonstrating the feasibility of an alternative solution: the relatively easy postprocessing of existing MRI datasets and subsequent calculation of the T1w/T2w ratio. This approach provides a pragmatic and efficient means to gain more realistic insights into focal alterations of myelin content. By leveraging widely available T1w and T2w sequences, we were able to obtain valuable information about myelin content without prolonging the scanning process or introducing additional specialized sequences.

In conclusion, our research highlights the significance of the T1w/T2w ratio as a practical and informative means to assess myelin content in the brain indirectly. By examining the T1w/T2w ratio compared to quantitative T1 mapping, we have demonstrated the feasibility of using standard MRI sequences to evaluate myelin levels indirectly. The utilization of standard MRI sequences makes this technique readily applicable to routine brain scans, providing a valuable tool for researchers and clinicians to investigate myelin-related conditions even in situations when specialized imaging protocols are not available and without extending the scanning duration, a crucial consideration, especially for pediatric patients.

## Conflict of Interest

There is no conflict of interest.

## Acknowledgements

We acknowledge with gratitude the funding support from the Czech Health Research Council, grant number NU21-08-00228, which enabled the realization of this research. Additionally, we would like to thank Veronika Borovcová and Jan Brhel for their exceptional skills as radiological assistants, demonstrating professionalism and expertise that greatly benefited our study.

## Abbreviations

T1w – T1 weighted image, T2w – T2 weighted image, qT1 – quantitative T1 image, MR – magnetic resonance, MRI – magnetic Resonance Imaging, dMRI – diffusion magnetic resonance imaging, MCD – malformations of cortical development, FCD – focal cortical dysplasia,

AEDs – available antiepileptic drugs, DKI – diffusion kurtosis imaging, FLAIR – fluid attenuated inversion recovery, DNET – dysembryoplastic neuroepithelial tumor, ROI – region of interest, ipsi – ipsilateral hemisphere, contra – contralateral hemisphere, FSL – FMRIB Software Library, SPM – Statistical Parametric Mapping software toolbox, MNI152 – Montreal Neurological Institute template, iOS – iPhone operating system, WM – white matter, GM – gray matter, CSF – cerebrospinal fluid, PET – positron emission tomography, LEAT – Long-term Epilepsy Associated Tumor, ILAE – International League Against Epilepsy, OLCs – oligodendrocyte-like cells, r – Spearman's rank correlation coefficient, a.u. – arbitrary units, 3D TSE – 3D turbo spin-echo, 3D MPRAGE – 3D Magnetization Prepared RApid Gradient Echo, EPI – Echo Planar Imaging.

## References

- Chang WC, Kudlacek J, Hlinka J, Chvojka J, Hadrava M, Kumpost V, Powell AD, ET AL. Loss of neuronal network resilience precedes seizures and determines the ictogenic nature of interictal synaptic perturbations. *Nat Neurosci* 2018;21:1742-1752. <https://doi.org/10.1038/s41593-018-0278-y>
- Noda AH, Hermsen A, Berkenfeld R, Dennig D, Endrass G, Kaltofen J, Safavi A, ET AL. Evaluation of costs of epilepsy using an electronic practice management software in Germany. *Seizure* 2015;26:49-55. <https://doi.org/10.1016/j.seizure.2015.01.010>
- West S, Nolan SJ, Cotton J, Gandhi S, Weston J, Sudan A, Ramirez R, Newton R. Surgery for epilepsy. *Cochrane Database Syst Rev* 2015;(7):CD010541. <https://doi.org/10.1002/14651858.CD010541.pub2>
- Blümcke I, Spreafico R, Haaker G, Coras R, Kobow K, Bien CG, Pfäfflin M, ET AL. Histopathological findings in brain tissue obtained during epilepsy surgery. *New Engl J Med* 2017;377:1648-1656. <https://doi.org/10.1056/NEJMoa1703784>
- Krsek P, Maton B, Jayakar P, Dean P, Korman B, Rey G, Dunoyer C, ET AL. Incomplete resection of focal cortical dysplasia is the main predictor of poor postsurgical outcome. *Neurology* 2009;72:217-223. <https://doi.org/10.1212/01.wnl.0000334365.22854.d3>
- Blümcke I, Thom M, Aronica E, Armstrong DD, Vinters HV, Palmini A, Jacques TS, ET AL. The clinicopathologic spectrum of focal cortical dysplasias: a consensus classification proposed by an ad hoc Task Force of the ILAE Diagnostic Methods Commission. *Epilepsia* 2011;52:158-174. <https://doi.org/10.1111/j.1528-1167.2010.02777.x>
- Krsek P, Pieper T, Karlmeier A, Hildebrandt M, Kolodziejczyk D, Winkler P, Pauli E, ET AL. Different presurgical characteristics and seizure outcomes in children with focal cortical dysplasia type I or II. *Epilepsia* 2009;50:125-137. <https://doi.org/10.1111/j.1528-1167.2008.01682.x>
- Kreilkamp BAK, Das K, Wiesmann UC, Biswas S, Marson AG, Keller SS. Neuroradiological findings in patients with "non-lesional" focal epilepsy revealed by research protocol. *Clin Radiol* 2018;74:78.e1-78.e11. <https://doi.org/10.1016/j.crad.2018.08.013>
- Wong-Kisiel LC, Blauwblomme T, Ho ML, Boddaert N, Parisi J, Wirrell E, Nababout R. Challenges in managing epilepsy associated with focal cortical dysplasia in children. *Epilepsy Res* 2018;145:1-17. <https://doi.org/10.1016/j.eplepsyres.2018.05.006>

10. Shepherd C, Liu J, Goc J, Martinian L, Jacques TS, Sisodiya SM, Thom M. A quantitative study of white matter hypomyelination and oligodendroglial maturation in focal cortical dysplasia type II. *Epilepsia* 2013;54:898-908. <https://doi.org/10.1111/epi.12143>
11. Scholl T, Mühlbner A, Ricken G, Gruber V, Fabing A, Samueli S, Gröppel G, ET AL. Impaired oligodendroglial turnover is associated with myelin pathology in focal cortical dysplasia and tuberous sclerosis complex. *Brain Pathol* 2017;27:770-780. <https://doi.org/10.1111/bpa.12452>
12. van der Weijden CWJ, García DV, Borra RJH, Thurner P, Meilof JF, van Laar P-J, Dierckx RAJO, ET AL. Myelin quantification with MRI: A systematic review of accuracy and reproducibility. *Neuroimage* 2021;226:117561. <https://doi.org/10.1016/j.neuroimage.2020.117561>
13. Kynčl M, Holubová Z, Tintěra J, Profantova N, Šanda J, Kala D, Prysiashniuk Y, ET AL. Recommendations for structural brain MRI in the diagnosis of epilepsy. *Ceska a Slovenska Neurologie a Neurochirurgie* 2023;86:18-24.
14. Ganzetti M, Wenderoth N, Mantini D. Whole brain myelin mapping using T1- and T2-weighted MR imaging data. *Front Hum Neurosci* 2014;8:671. <https://doi.org/10.3389/fnhum.2014.00671>
15. Ganzetti M, Wenderoth N, Mantini D. Mapping pathological changes in brain structure by combining T1- and T2-weighted MR imaging data. *Neuroradiology* 2015;57:917. <https://doi.org/10.1007/s00234-015-1550-4>
16. Iwatani J, Ishida T, Donishi T, Ukai S, Shinosaki K, Terada M, Kaneoke Y. Use of T1-weighted/T2-weighted magnetic resonance ratio images to elucidate changes in the schizophrenic brain. *Brain Behav* 2015;5:399. <https://doi.org/10.1002/brb3.399>
17. Chen H, Budin F, Noel J, Prieto JC, Gilmore J, Rasmussen J, Wadhwa PD, ET AL. White matter fiber-based analysis of T1w/T2w ratio map. *Proc SPIE Int Soc Opt Eng* 2017;10133:101330P. <https://doi.org/10.1117/12.2254467>
18. Scott KT. SPACE: An Innovative Solution to Rapid, Low SAR, T2-Weighted Contrast in 3D Spin Echo Imaging. Siemens Medical Solutions. Published online 2009.
19. Henschel L, Conjeti S, Estrada S, Diers K, Fischl B, Reuter M. FastSurfer - A fast and accurate deep learning based neuroimaging pipeline. *Neuroimage* 2020;219:117012. <https://doi.org/10.1016/j.neuroimage.2020.117012>
20. Kazemi K, Noorizadeh N. Quantitative Comparison of SPM, FSL, and Brainsuite for Brain MR Image Segmentation. *J Biomed Phys Eng* 2014;4:13-26.
21. Glasser MF, van Essen DC. Mapping Human Cortical Areas In Vivo Based on Myelin Content as Revealed by T1- and T2-Weighted MRI. *J Neurosci* 2011;31:11597-11616. <https://doi.org/10.1523/JNEUROSCI.2180-11.2011>
22. Uddin MN, Figley TD, Marrie RA, Figley CR. Can T1w/T2w ratio be used as a myelin-specific measure in subcortical structures? Comparisons between FSE-based T1w/T2w ratios, GRASE-based T1w/T2w ratios and multi-echo GRASE-based myelin water fractions. *NMR Biomed* 2018;31:e3868. <https://doi.org/10.1002/nbm.3868>
23. Margaret Cheng HL, Stikov N, Ghugre NR, Wright GA. Practical medical applications of quantitative MR relaxometry. *J Magn Reson Imaging* 2012;36:805-824. <https://doi.org/10.1002/jmri.23718>
24. Luzzi S, Elia A, Del Maestro M, Elbabaa SK, Carnevale S, Guerrini F, Caulo M, ET AL. Dysembryoplastic Neuroepithelial Tumors: What You Need to Know. *World Neurosurg* 2019;127:255-265. <https://doi.org/10.1016/j.wneu.2019.04.056>
25. Scelsi CL, Rahim TA, Morris JA, Kramer GJ, Gilbert BC, Forseen SE. The Lateral Ventricles: A Detailed Review of Anatomy, Development, and Anatomic Variations. *AJNR Am J Neuroradiol* 2020;41:566-572. <https://doi.org/10.3174/ajnr.A6456>
26. Piredda GF, Hilbert T, Thiran JP, Kober T. Probing myelin content of the human brain with MRI: A review. *Magn Reson Med* 2021;85:627-652. <https://doi.org/10.1002/mrm.28509>
27. Kala D, Šulc V, Olšerová A, Svoboda J, Prysiashniuk Y, Poštusta A, Kynčl M, ET AL. Evaluation of blood-brain barrier integrity by the analysis of dynamic contrast-enhanced MRI - a comparison of quantitative and semi-quantitative methods. *Physiol Res* 2022;71(Suppl 2):S259-S275. <https://doi.org/10.33549/physiolres.934998>